Kinetic Mechanism of MyosinV-S1 Using a New Fluorescent ATP Analogue[†]

Eva Forgacs,[‡] Suzanne Cartwright,[‡] Mihály Kovács,[§,‖] Takeshi Sakamoto,[§] James R. Sellers,[§] John E. T. Corrie,[⊥] Martin R. Webb,[⊥] and Howard D. White*,[‡]

Department of Physiological Sciences, Eastern Virginia Medical School, Norfolk, Virginia 23507,
MRC National Institute for Medical Research, Mill Hill, London, NW7 1AA, United Kingdom,
Laboratory of Molecular Physiology, National Heart, Lung and Blood Institute, Bethesda, Maryland 20892-1762,
and Department of Biochemistry, Eötvös University, Pázmány stny.1/c, H-1117 Budapest, Hungary

Received April 12, 2006; Revised Manuscript Received August 11, 2006

ABSTRACT: We have used a new fluorescent ATP analogue, 3′-(7-diethylaminocoumarin-3-carbonylamino)-3′-deoxyadenosine-5′-triphosphate (deac-aminoATP), to study the ATP hydrolysis mechanism of the single headed myosinV-S1. Our study demonstrates that deac-aminoATP is an excellent substrate for these studies. Although the deac-amino nucleotides have a low quantum yield in free solution, there is a very large increase in fluorescence emission ($\sim$20-fold) upon binding to the myosinV active site. The fluorescence emission intensity is independent of the hydrolysis state of the nucleotide bound to myosinV-S1. The very good signal-to-noise ratio that is obtained with deac-amino nucleotides makes them excellent substrates for studying expressed proteins that can only be isolated in small quantities. The combination of the fast rate of binding and the favorable signal-to-noise ratio also allows deac-nucleotides to be used in chase experiments to determine the kinetics of ADP and Pi dissociation from actomyosin-ADP-Pi. Although phosphate dissociation from actomyosinV-ADP-Pi does not itself produce a fluorescence signal, it produces a lag in the signal for deac-aminoADP dissociation. The lag provides direct evidence that the principal pathway of product dissociation from actomyosinV-ADP-Pi is an ordered mechanism in which phosphate precedes ADP. Although the mechanism of hydrolysis of deac-aminoATP by (acto)myosinV-S1 is qualitatively similar to the ATP hydrolysis mechanism, there are significant differences in some of the rate constants. Deac-aminoATP binds 3-fold faster to myosinV-S1, and the rate of deac-aminoADP dissociation from actomyosinV-S1 is 20-fold slower. Deac-aminoATP supports motility by myosinV-HMM on actin at a rate consistent with the slower rate of deac-aminoADP dissociation.

Actomyosin motors play a pivotal role in many cellular functions such as cellular transport, muscle contraction, and cell motility. The energy source of these cellular motor proteins is ATP hydrolysis. Actomyosin proceeds through a series of intermediates during the ATP hydrolysis cycle, which modulates the protein conformation and the interaction between actin and myosin. Several fluorescent ATP analogues such as ϵATP (*1*), azaATP (*2*), mantATP (*3*), deoxymant ATP (*4*), Cy3ATP, and Cy5ATP (*5*) have been used to aid in understanding the relationship between the ATP hydrolysis mechanism and the chemomechanical transduction. Nucleotides in which a fluorescent group is covalently linked to the 3′- and/or 2′-position of the ribose have proven especially useful, as they have a hydrolysis mech-

anism similar to ATP and a fluorescence emission that is sensitive to the altered environment produced upon binding to the active site of myosin (e.g., a 2-fold enhancement in emission with mant and deoxymantATP). A recent addition to the 3′-fluorescent ATP derivatives is deac-aminoATP,[1] in which the coumarin is coupled to 3′-amino-3′-deoxyATP by an amide linkage to produce a single, stable isomer. The increase in the fluorescence emission observed when deac-aminoATP or deac-aminoADP binds to skeletal myosinII is the largest ($\sim$20-fold) of any of the nucleotide analogues tested to date. Measurements of the steady-state rate of deac-aminoATP hydrolysis and the rate of deac-aminoADP dissociation from rabbit skeletal actomyosin suggest that the hydrolysis mechanism is similar to that of the natural substrate, ATP (*6*). We have therefore made a detailed study of the mechanism of hydrolysis of deac-aminoATP by myosinV-S1 to determine if there are any significant changes

* Corresponding author. Phone: (757) 446-5652; fax: (757) 624-2270; e-mail: whitehd@evms.edu.
‡ Eastern Virginia Medical School.
§ National Heart, Lung and Blood Institute.
‖ Eötvös University.
⊥ MRC National Institute for Medical Research.

[1] Abbreviations: actin, filamentous actin; myosinV-S1, myosinV subfragment 1; myosinV-HMM, heavy meromyosinV.; deac-aminoATP, 3′-(7-diethylaminocoumarin-3-carbonylamino)-3′-deoxyadenosine-5′-triphosphate; ϵATP, 1,N^6-ethenoadenosine-5′-triphosphate; azaATP, 1,N^6-etheno-2-aza-ATP.; mantATP, 2′(3′)-*O*-(*N*-methylanthraniloyl)-adenosine-5′-triphosphate; deoxymantATP, 2′-deoxy-3′-mantATP; cy3ATP, 2′(3′)-*O*-[*N*-2-(Cy3-amino)ethyl]carbamoyl]adenosine-5′-triphosphate; cy5ATP, 2′(3′)-*O*-[*N*-2-(Cy5-amino)ethyl]carbamoyl]-adenosine 5′-triphosphate; MDCC-PBP, *N*-[2-(1-maleimidyl)ethyl]-7-diethylaminocoumarin-3-carboxamide labeled phosphate-binding protein.
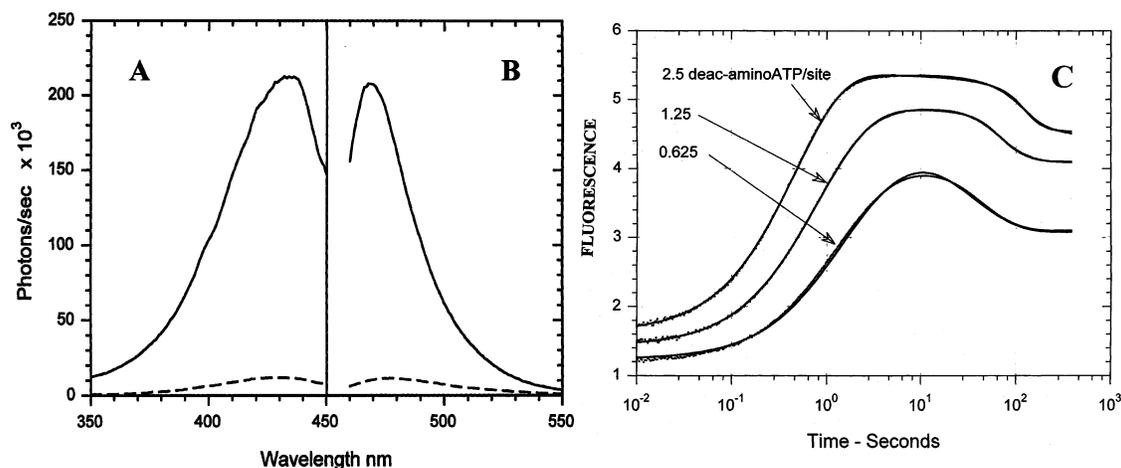
FIGURE 1: Excitation and emission spectra of deac-aminoADP and myosinV-S1-deac-aminoADP and active site titration of myosinV-S1 with deac-aminoATP. Excitation (A) and emission (B) spectra of 0.5 μM deac-aminoADP were taken in the absence (dashed lines) and presence (solid lines) of 1.0 μM myosinV-S1. Excitation spectra were taken using an emission wavelength of 430 nm, and excitation spectra were taken at an emission wavelength of 470 nm. Experimental conditions: 10 mM MOPS, 25 mM KCl, 3 mM MgCl$_2$, 1 mM EGTA, pH 7.5 at 20 °C. (C) MyosinV-S1 was mixed with deac-aminoATP to give final concentrations in the cell of 0.27 μM myosinV-S1 and either 0.17, 0.34, or 0.68 μM deac-aminoATP in the same buffer as in panel A. The lines through the data are global fits to rate constants k_T, 3.4×10^6 M^{-1}s^{-1}; k_{-P}, 0.025 s^{-1}; $1/K_D$, 0.1 μM (see eq 1 in text); and an active site concentration of 0.23 μM.

in the hydrolysis mechanism by myosinV and to explore the utility of deac-aminoATP for making kinetic studies of some of the recombinant and tissue purified myosins that are available only in small quantities. This work will also provide a baseline of kinetic values of the mechanism of hydrolysis of deac-aminoATP by single headed myosinV-S1 for comparison with studies using deac-aminoATP to measure the interaction between the two heads of myosinV-HMM. The large signals produced upon deac-aminoATP binding and deac-aminoADP dissociation to/from skeletal myosinII suggest that this nucleotide analogue would be ideal for kinetic measurements utilizing small amounts of proteins, such as recombinant myosinV.

MyosinV is a two-headed actin-based motor (*7−10*) that has been shown to move processively on the actin filament (*8, 11−15*). The processivity has been proposed to occur by a gating mechanism, which ensures that one head of the molecule always remains attached to the actin (*16*). Kinetic studies of the single headed myosinV-S1 show that, although the overall ATP hydrolysis mechanism is similar to that of muscle myosin, there are key differences: ADP dissociation is the slowest step of the ATPase mechanism, and myosinV has a much higher affinity than myosinII for actin in the presence of ATP. As a result of these kinetic properties, myosinV is a high duty cycle motor and spends a large fraction of the hydrolysis cycle strongly bound to actin (*15, 17*). The high duty cycle of myosinV is in contrast with that of muscle myosins, which spend less than 20% of the time bound to actin within the hydrolytic cycle and undergo a cycle of attachment and detachment with each molecule of ATP hydrolyzed (*18, 19*). Here, we have determined the kinetic mechanism of actomyosinV-S1 ATP hydrolysis using the fluorescent analogue 3′-deac-aminoATP (*6*). The fluorescence enhancement observed when deac-aminoATP and deac-aminoADP are bound to myosinV-S1 is similar to that observed upon binding to myosinII-S1, ~20-fold. This is 10-fold greater than the enhancement observed upon mant and deoxymant nucleotide binding to the active site (*20*). The very large fluorescent enhancement that occurs upon binding of this nucleotide to the active site of myosin enables

it to be used to determine the active site concentration accurately with as little as 10 pmol of myosin active sites. It also enables deac-aminoATP or deac-aminoADP to be used as a chase at concentrations as large as 100 times the active site concentration and still obtain very good signal-to-noise ratios. Although the fluorescence enhancement is not measureably different for deac-aminoATP, deac-aminoADP-Pi, or deac-aminoADP bound to the active site of (acto)-myosinV-S1, the good signal-to-noise ratio enables phosphate dissociation from actomyosinV-deac-aminoADP-Pi to be observed from the lag in the fluorescent signal that is produced by the dissociation of phosphate. The 20-fold slower rate of dissociation of deac-aminoADP than ADP from actomyosinV-S1 can be compared to the 20-fold slower velocity observed using the in vitro motility measurements with deac-aminoATP as compared to ATP. This provides additional evidence that ADP dissociation is the rate-limiting step for myosinV movement.

EXPERIMENTAL PROCEDURES

Preparations of MyosinV-S1. Mouse myosinV-S1 heavy chain, 907 amino acid residues including 6IQ domains, or myosin V-HMM, 1090 amino acid residues, were coexpressed with calmodulin in a baculovirus/Sf9 cell system. The proteins were purified using FLAG-affinity chromatography (*21*) and then concentrated and fractionated on a MonoQ ion-exchange column with a linear gradient of 0.1−0.5 M NaCl in 10 mM MOPS, 0.1 mM EGTA, 3 mM NaN$_3$, and 1 mM DTT, pH 7.2, using HPLC. The concentration of myosinV-S1 was determined from the A$_{280}$ after correction for light scattering (A$_{280}$−1.5A$_{320}$). The extinction coefficient was calculated to be 1.1×10^5 M^{-1} cm^{-1} from the number of tyrosine and tryptophan residues and their molar extinction coefficients: $\epsilon = (n = 10)_{trp} \times 5690 + (n = 42)_{tyr} \times 1280$ (*22*). All preparations were analyzed by SDS protein gel electrophoresis and by active site titration with deac-aminoATP as shown in Figure 1C.

Reagents. Actin was purified from rabbit skeletal muscle (*23*). ATP and ADP were purchased from Sigma-Aldrich.

MDCC-PBP was prepared according to Brune et al. (*24*). Deac-aminoATP and deac-aminoADP were synthesized by Webb et al. (*6*). Deac-amino nucleotide concentrations were based upon molar extinction coefficients of the deac-aminoATP and deac-aminoADP, $\epsilon_{429} = 46\,800$ M^{-1} cm^{-1}.

Steady-State Fluorescence Spectra. Excitation and emission spectra were taken with a PTI MD5020 photon-counting spectrofluorimeter with thermostated cell housing. Excitation was provided by a 75 W xenon arc lamp and a 20 cm monochromator with a 4 nm slit width. Buffer blanks were subtracted from all spectra.

Stopped-Flow Measurements. All measurements were done in an SF-2001 stopped-flow apparatus (Kintek Corp., Austin, TX). Unless otherwise stated, all experiments were in a buffer containing 10 mM MOPS, 3 mM $MgCl_2$, 25 mM KCl, and 1 mM EGTA, pH 7.5 at 20 °C. Deac-aminoATP, deac-aminoADP, and MDCC-PBP were excited at 430 nm, and the emitted light was selected using a 450 nm long pass sharp cutoff filter. Pi dissociation from the actomyosinV-S1-ADP-Pi complex was measured using MDCC-PBP as described (*25*). Background Pi was removed by preincubating the stopped-flow apparatus and all working solutions with the phosphate mop consisting of 0.1 mM 7-methylguanosine and 0.01 units/mL purine-nucleoside phosphorylase (*26*). Actin concentrations <5 μM were stabilized with equimolar concentrations of phalloidin.

Steady-State Basal and Actin-Activated ATPase Measurements. Steady-state ATPase activities were measured by an NADH-coupled assay at 25 °C in buffer containing 10 mM MOPS (pH 7.0), 2 mM $MgCl_2$, 50 mM KCl, 0.15 mM EGTA, 1 mM ATP, 40 units/mL lactate dehydrogenase, 200 units/mL pyruvate kinase, 1 mM phosphoenolpyruvate, and 200 μM NADH. Changes in NADH absorption at 340 nm ($\epsilon = 6220$ M^{-1} cm^{-1}) were followed in a Beckman DU640 spectrophotometer. The ATPase activity of blanks containing actin but no myosin was subtracted from the actomyosin data.

In Vitro Motility Assays. In vitro actin gliding assays at 30 °C using myosinV-HMM were performed as described previously in a buffer containing 20 mM MOPS (pH 7.5), 5 mM $MgCl_2$, 0.1 mM EGTA, 50 mM KCl, 50 mM dithiothreitol, various concentrations of ATP or deac-aminoATP, and an oxygen scavenging system consisting of 2.5 mg/mL glucose, 0.1 mg/mL glucose oxidase, and 2 μg/mL catalase (*27*). Actin filaments were labeled with rhodamine−phalloidin. All motility assays were performed on an Olympus IX70 microscope with an objective-type TIRF system and excitation light sources as previously described (*13*). To acquire images, time-lapse data collection was used in which the field was only illuminated every 100 s for a 20 ms period to prevent photobleaching of the fluorescence. The velocity of individual actin filaments was calculated using the Track Objects function of Metamorph software (Advanced Microdevices).
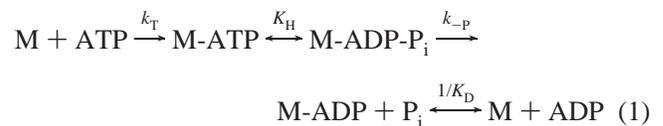
Data Analysis and Kinetic Simulation. Scientist software (*28*) and the Kintek SF-2001 software were used for data fitting and kinetic modeling.

RESULTS

Excitation and Emission Spectra of Deac-aminoADP in the Presence and Absence of MyosinV-S1. The emission of deac-aminoADP was increased approximately 20-fold when bound to the active site of myosinV-S1 as shown by the excitation and emission spectra in Figure 1A,B. There are small shifts in the excitation maximum from 430 to 432 nm and in the excitation maximum from 475 to 470 nm in the emission maximum when deac-aminoADP is bound to myosinV-S1, but the predominant feature of the spectral change is the very large ∼20-fold increase in the emission intensity. A similar increase was observed when deac-aminoADP was bound to skeletal myosin-S1 (*6*).

Deac-aminoATP Binding to MyosinV-S1 (Active Site Titration). We have conducted single turnover stopped-flow measurements of the hydrolysis of deac-aminoATP to determine the active site concentrations of the myosinV-S1. The fluorescence enhancement observed upon mixing deac-aminoATP from ∼0.5 to 2 times the active site concentration with myosinV-S1 is shown in Figure 1C. At substoichiometric deac-aminoATP concentrations (lowest curve), the fluorescence increased to a maximum as the nucleotide bound and then slowly decreased to a constant value as the myosinV-S1-deac-aminoADP-Pi complex dissociates. With excess deac-aminoATP concentrations (upper curves), a steady-state level of fluorescence enhancement occurred after binding was complete, which was then followed by a decrease to a constant value. The decrease in the fluorescence was produced by partial dissociation of deac-aminoADP in which the rate was limited by the slow dissociation of phosphate. The data can be accurately described by global fits of the fluorescence to eq 1 to determine the active site concentration of myosinV-S1, the rate constant of deac-aminoATP binding (k_T), the phosphate release rate constant (k_{-P}), and the equilibrium constant of deac-aminoADP binding (K_D). A value of 5 for K_H was determined by quench−flow under the same experimental conditions (data not shown) and was fixed during the fitting. Fitting was done to differential equations describing the following mechanism using the simplex fitting algorithm in the Scientist package (*28*).

$$M + ATP \xrightarrow{k_T} M\text{-}ATP \xleftrightarrow{K_H} M\text{-}ADP\text{-}P_i \xrightarrow{k_{-P}}$$

$$M\text{-}ADP + P_i \xleftrightarrow{1/K_D} M + ADP \quad (1)$$

The active site concentration, determined in Figure 1B, is 0.23 μM, 85% of the value of 0.27 μM, which was determined from A_{280} and the extinction coefficient of myosinV-S1. The stoichiometry in all myosinV-S1 preparations was in the range of 0.85−0.95. The second-order rate constant for deac-aminoATP binding was 3.5×10^6 M^{-1} s^{-1}, which is ∼3 times the rate measured for the binding of ATP and mantATP to myosinV-S1 (*15*, *17*). The fitted phosphate release rate constant, 0.025 s^{-1}, is similar to the steady-state rate obtained with either ATP or mantATP substrates. The affinity of deac-aminoADP for myosinV-S1, ∼0.1 μM, is approximately 3 times higher than the affinity of deoxymant-ADP for myosinV-S1 (*15*). Although four parameters were varied during the fitting, (k_T, k_{-P}, K_D, and [M]), it produced a robust fit that independently determined the values of the parameters.

Steady-State ATPase Activity. The basal and actin-activated ATPase activities of myosinV-S1 with deac-aminoATP as the substrate were measured with a NADH-coupled ATP-regenerating system (*29*). The hydrolysis rates were deter-
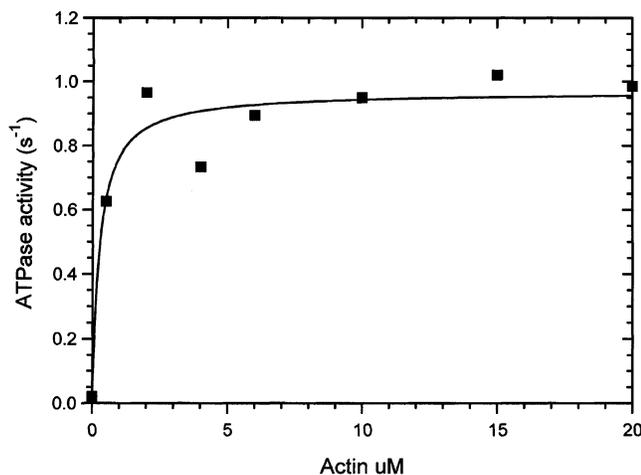
FIGURE 2: Steady-state deac-aminoATP hydrolysis. Steady-state deac-aminoATPase activites were measured by an NADH-coupled assay described in the Experimental Procedures. 0.1 μM deac-aminoATP and either 0.25 μM myosinV-S1 (basal) or 0.01 μM myosinV-S1 and the indicated concentrations of phalloidin actin were used at 25 °C. The data points represent averages of two sets of experiments. The solid line through the data is a fit to the curve $k_{obs} = (k_{max}/(1 + K_{app}/[actin])) + k_o$, where $k_{max} = 0.86$ s^{-1}, $K_{app} = 0.12$ μM, and $k_o = 0.025$ s^{-1}.

mined from the change in absorption at 340 nm, which was linear between 1 and 30 min after initiating the reaction. Identical results were obtained when the reaction was initiated by the addition of either myosinV-S1 or deac-aminoATP. The steady-state deac-aminoATPase activity increased from a basal rate of 0.025 s^{-1} to a maximum actin-activated rate of 0.86 s^{-1} at 25 °C (Figure 2). The maximum rate can be compared with the rate of deac-aminoADP dissociation from actomyosinV-S1-deac-aminoADP-Pi of 0.52 s^{-1} at 20 °C (Figure 4) and 0.75 s^{-1} at 25 °C (data not shown). The good agreement between the rate of deac-aminoADP dissociation, 0.75 s^{-1}, and the rate of maximum-activated ATPase, 0.86 s^{-1}, provides evidence that deac-aminoADP dissociation is the rate-limiting step. Higher concentrations of deac-aminoATP inhibit the steady-state hydrolysis rate both in the presence and in the absence of actin, even in the presence of the regenerating system (data not shown). We determined the activity of the deac-aminoATP regenerating system using skeletal actomyosin-S1 and 5 μM deac-aminoATP and found that the regenerating system can measure a steady-state hydrolysis rate of at least 5 s^{-1}. The inhibition of basal and actin-activated deac-aminoATPase activities at high deac-aminoATP concentrations indicates that the regenerating system works well enough with deac-aminoADP to follow the hydrolysis but does not keep the deac-aminoADP concentration low enough to prevent it from being a competitive inhibitor of deac-aminoATP binding to actomyosinV. This is consistent with the high affinities (~0.1 μM) of deac-aminoADP for myosinV-S1 and actomyosinV-S1 measured in Figures 1 and 4, which predict that deac-aminoADP should be a very good competitive inhibitor. It has previously been shown that ADP, which binds less tightly to myosinV-S1 than deac-aminoADP, is also a potent competitive inhibitor of myosinV ATP hydrolysis (*30*).

Deac-aminoATP Binding to ActomyosinV-S1. The fluorescence enhancement observed with deac-aminoATP binding to actomyosinV-S1 in a single mixing stopped-flow

experiment is shown in Figure 3A. The fast phase of the increase was associated with the major component of the fluorescence enhancement (~95% of the amplitude) and was dependent upon the deac-aminoATP concentration with a maximum rate of 207 ± 20 s^{-1} and a K_{app} of 60 ± 5 μM (Figure 3B). The slow phase of the fluorescence enhancement changed linearly with the deac-aminoATP concentration and had an apparent second-order rate constant of 4×10^4 M^{-1} s^{-1}. The significance of the low amplitude slow phase of the fluorescence enhancement is not clear. It is unlikely to be due to contaminating ADP bound to the active sites as the rate is 5–10 times slower than the rate of ADP dissociation from actomyosinV-S1. It is only rapid enough to be on the kinetic pathway of actomyosinV deac-aminoATP hydrolysis at high substrate concentrations as the steady-state rate is ~0.5 s^{-1}. It is possible that the slow component may represent a second conformation of myosin, myosin-deac-aminoATP, or a small percentage of myosin molecules that slowly bind the substrate. A component that produces such a small part of the fluorescent signal would be lost in the noise with other fluorescent nucleotide substrates and is only observable here because of the high signal-to-noise ratio of deac-aminoATP.

Deac-aminoADP Binding to and Dissociation from MyosinV-S1 and ActomyosinV-S1. The rates of deac-aminoADP binding to myosinV-S1 and to actomyosinV-S1 were measured by the fluorescence enhancement observed upon mixing either myosinV-S1 or actomyosinV-S1 with deac-aminoADP (Figure 4A,D). The data were best fit by double exponential time courses in which 90% of the fluorescence increase was fast and dependent upon the deac-aminoADP concentration (Figure 4B,E). The rate of the slow phase, 1 s^{-1}, is similar to that observed with deac-aminoATP and is independent of actin concentration. The second-order rate constants, 5.7 ± 0.2 μM^{-1} s^{-1} for myosinV-S1 and 5.4 ± 0.1 μM^{-1} s^{-1} for actomyosinV-S1, were determined from a linear fit of the dependence of the fast phase upon deac-aminoADP concentration. The dissociation rates are estimated from the *y* intercepts to be approximately 1.0 ± 0.2 s^{-1} for myosinV-S1 and 2.6 ± 0.7 s^{-1} for actomyosinV-S1 (Figure 4B,E). A more direct measurement of the rate of dissociation of deac-aminoADP was determined by mixing either myosinV-S1-deacADP or actomyosinV-S1-deac-aminoADP with an ATP chase, as shown in Figure 4C,F. The kinetics of deac-aminoADP dissociation was accurately fit by single exponentials with rate constants of 0.49 s^{-1} for myosinV-S1 and 0.52 s^{-1} for actomyosinV-S1. The equilibrium constants for deac-aminoADP binding can be calculated from the rates of binding and dissociation to be 0.09 μM for both myosinV-S1 (0.49 s^{-1}/5.4 μM^{-1} s^{-1}) and actomyosinV-S1 (0.52 s^{-1}/5.7 μM^{-1} s^{-1}). The value of 0.09 μM obtained from the rate constants for deac-aminoADP binding to myosinV-S1 is in good agreement with the value of 0.1 μM obtained by fitting the final fluorescence levels in single turnover experiments in Figure 1C. Although the second phase of the fluorescence signal observed during deac-aminoADP binding suggests an additional myosinV-S1-deacADP intermediate as has been observed for myosinV-S1 with mantADP (*31*), the near equality of the value for the equilibrium constant obtained at equilibrium in Figure 1C and by kinetic measurements in Figure 4 is consistent with there being predominantly single myosinV-S1-deac-
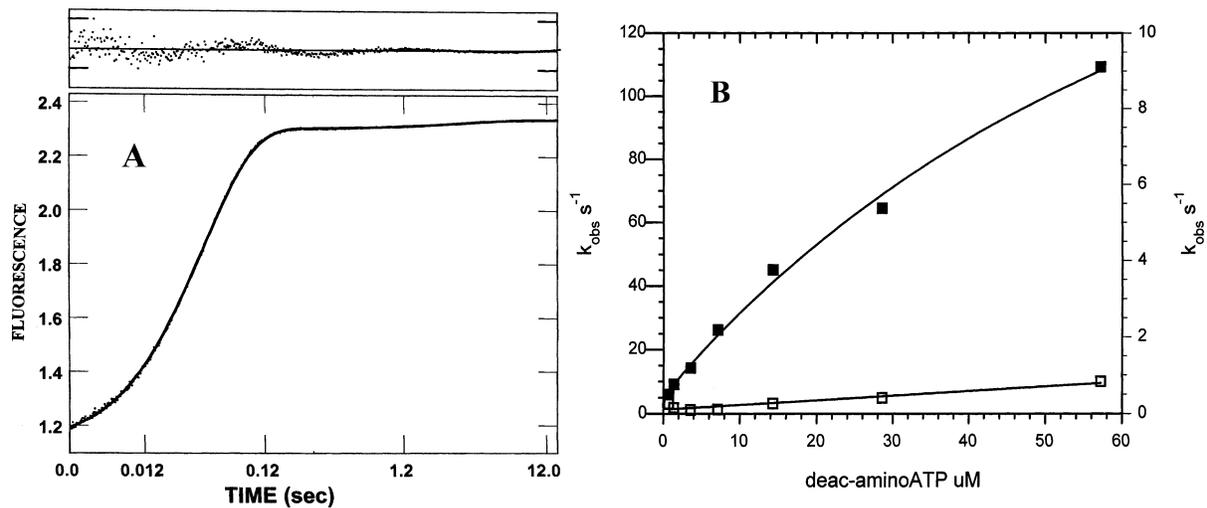
FIGURE 3: Deac-aminoATP binding to actomyosinV-S1. (A) Representative trace of a single mixing stopped flow experiment in which actomyosinV-S1 was mixed with deac-aminoATP. The solid line fit to the data is $I(t) = 1 - (0.95\ e^{-8.5t} + 0.05e^{-0.05t}) + C$. Experimental conditions in the flow cell were 1.4 μM actin, 0.14 μM myosinV-S1, 3.6 μM deac-aminoATP, 10 mM MOPS, 3 mM MgCl$_2$, 25 mM KCl, and 1 mM EGTA, pH 7.5, 20 °C. (B) Experimental conditions were the same as those described in panel A except that the deac-aminoATP concentrations were varied from 0.14 to 56 μM. The line through the solid symbols is a fit of the rapid phase of the fluorescence to the equation $k_{obs} = 207/(1 + 60/[\text{deac-aminoATP}])$. The line through the open symbols is a fit to the slow fluorescence increase and results in a second-order rate constant of 4×10^4 M^{-1}s^{-1}.

aminoADP and actomyosinV-S1-deac-aminoADP species. This is also consistent with the very accurate single exponential dissociation of deac-aminoADP from myosinV-S1 and actomyosinV-S1.

ADP Dissociation from MyosinV-S1-ADP and Actomyo-sinV-S1-ADP. The rates of ADP dissociation from myosinV-S1-ADP and actomyosinV-S1-ADP were measured by using deac-aminoADP as a chase in single mixing stopped-flow experiments. The data for both myosinV-S1-ADP and acto-myosinV-S1-ADP were best fit to double exponentials as shown in Figure 5A,B in which more than 90% of the signal was associated with the more rapid fluorescence change. For myosinV-S1-ADP, the dependence of the rates upon the deac-aminoADP concentration had a maximum rate of 5.9 ± 0.3 s^{-1} for the fast and 0.96 ± 0.5 s^{-1} for the slower phase (Figure 5C). The rate and fraction of the amplitude associated with the slow phase is similar to that observed for the binding of deac-aminoATP to myosinV-S1 in the absence of ADP in Figure 3. The slow phases, which were observed during deac-aminoADP binding to myosinV-S1 (Figure 4A), there-fore, cannot be due to ADP bound to a small fraction of the myosinV-S1 as the amplitudes and rates are unchanged by additionally bound ADP. The dependence of the rate of the fluorescence increase upon deac-aminoADP concentration with actomyosinV-S1-ADP is shown in Figure 5D. The solid line through the data corresponds to a maximum rate of 10.6 s^{-1} for the fast phase. The rates of fast phase components measured with a deac-aminoADP chase in Figure 5 cor-respond well with the previously measured rates of ADP dissociation from mouse and chicken myosinV-S1 and actomyosinV-S1 using mant nucleotides as a chase (*15, 17*). The rate of the slow components is similar to those measured for the binding of deac-aminoADP to myosinV-S1 and actomyosinV-S1 in Figure 4. This slow phase is therefore likely to represent a conformational equilibrium between (acto)myosinV-S1-deac-aminoADP states rather than be-tween (acto)myosinV-ADP states.

Measurement of ADP and Phosphate Release from the MyosinV-S1-deac-aminoADP-Pi Complex. We used double

mixing stopped-flow experiments to measure the rate of the product release steps using deac-aminoATP as the substrate. Equimolar concentrations of myosinV-S1 and deac-amino-ATP were mixed, and the reaction aged for 20 s to allow deac-aminoATP to bind and be hydrolyzed by myosinV-S1. The kinetics of product dissociation were measured after a second mix with actin and a 200 μM ATP chase to prevent deac-aminoADP rebinding. In the absence of actin, the rate of product dissociation was 90% of the total intensity at 0.025 s^{-1} and 10% at 0.5 s^{-1}, as expected from the steady-state rate and the rate of deac-aminoADP dissociation determined in Figures 1C and 4. In the presence of 0.25–20 μM actin, the fluorescence was fit well by a rate constant of 0.51 ± 0.02 s^{-1}, which was independent of actin concentration in the low salt (25 mM KCl) buffer conditions (data not shown). These data indicate that the second-order rate constant of actin binding to and acceleration of phosphate dissociation from myosinV-S1-deacADP-Pi is greater than (0.5 s^{-1}/0.25 μM) $\sim$2 $\times$ 10^6 M^{-1} s^{-1}. Since binding of most myosins to actin is less rapid at higher ionic strength, we repeated the same experiments with 100 mM KCl. As expected, at the higher salt concentration, the kinetics of product dissociation at low actin concentrations were slower and dependent upon the actin concentration (Figure 6A). Moreover, at actin concentrations in the range of 0.5–4 μM, the fluorescence signal is not fit well by a single exponential (dashed lines, Figure 6A). However, the data are fit well by a two-exponential equation in which the amplitudes have opposite signs, the mathematical form of a lag (solid line, Figure 6A). The dependence of the two rates upon actin concentrations is shown by the closed and open squares in Figure 6C. One exponential term shows a hyperbolic dependence upon actin concentration with a maximum rate of 0.70 ± 0.01 s^{-1}. The second exponential term is linear with an actin concentration over the range that is measurable and has an apparent second-order rate constant of 6 $\times$ 10^5 M^{-1} s^{-1}. The dependence of the rate and amplitudes upon actin concentration is that predicted by an ordered mechanism in which phosphate dissociation from actomyosin-deac-
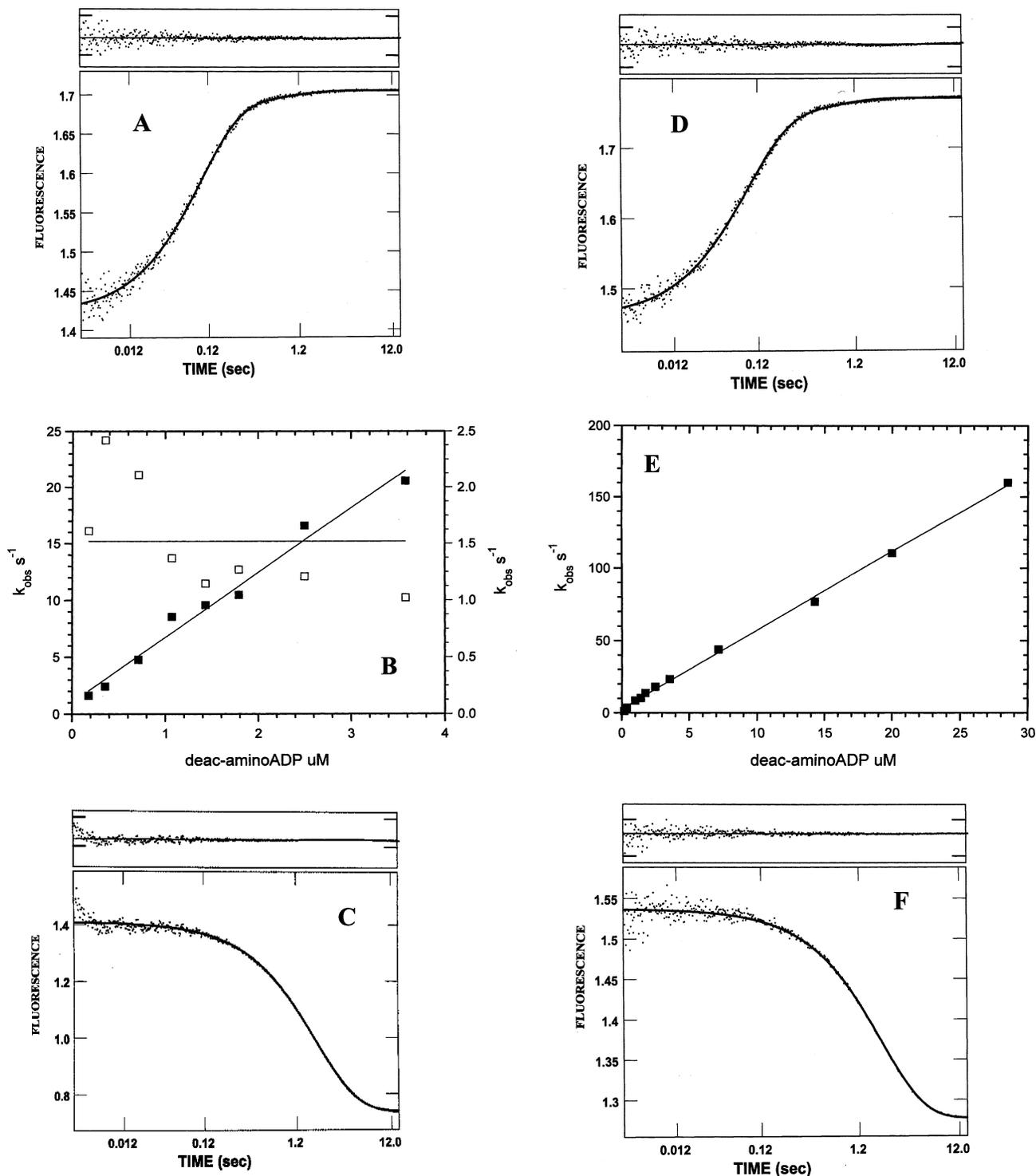
FIGURE 4: Deac-aminoADP binding to and dissociation from myosinV-S1 (A–C) and actomyosinV-S1 (D–F). (A) Time course of the fluorescence increase observed upon deac-aminoADP binding to myosinV-S1 (A). Final concentrations in the flow cell were 1.42 μM deac-aminoADP and 0.074 μM myosinV-S1. The data are fit to a double exponential equation with normalized amplitudes: $I(t) = 1 - (0.96e^{-9.6t} + 0.04e^{-1.1t}) + C$. (B) Deac-aminoADP dependence of the myosinV-S1-binding kinetics. Experimental conditions were similar to those described in panel A except that the final deac-aminoADP concentration in the flow cell was varied as indicated: the line through the fast phase (■) was fit to a straight line corresponding to a second-order rate constant of $k_{AD} = 5.7 \pm 0.1$ μM^{-1} s^{-1}. The slow phase (□) was fit to an actin independent rate of 1.5 s^{-1}. (C) Time course of deac-aminoADP dissociation from myosinV-S1-deac-aminoADP. Final concentrations in the flow cell were 0.057 μM myosinV-S1, 0.57 μM deac-aminoADP, and 143 μM ATP in MOPS buffer containing 25 mM KCl at 20 °C. The data are fit to a single exponential with a k_{obs} of 0.49 s^{-1}. (D) Time course of the fluorescence increase observed with deac-aminoADP binding to actomyosinV-S1. Final concentrations in the flow cell were 1.0 μM deac-aminoADP, 0.04 μM myosinV-S1, and 0.4 μM actin. The data are fit to a double exponential equation (normalized amplitudes): $I(t) = 1 - (0.9e^{-10.2t} + 0.1e^{-1.1t}) + C$. (E) Dependence of the kinetics of deac-aminoADP binding to actomyosinV-S1 upon different deac-aminoADP concentrations. Final concentrations in the flow cell were the same as panel D except that deac-aminoADP was varied as indicated. The k_{obs} were determined from the fast component of panel D. The second-order rate constant was determined from the slope $k_{AD} = 5.4 \pm 0.1$ μM^{-1} s^{-1}. (F) Time course of deac-aminoADP dissociation from actomyosinV-S1. Experimental conditions were the same as those described in panel C except that 1.42 μM phalloidin actin was present in the flow cell. The data are fit with a k_{obs} of 0.52 s^{-1}.
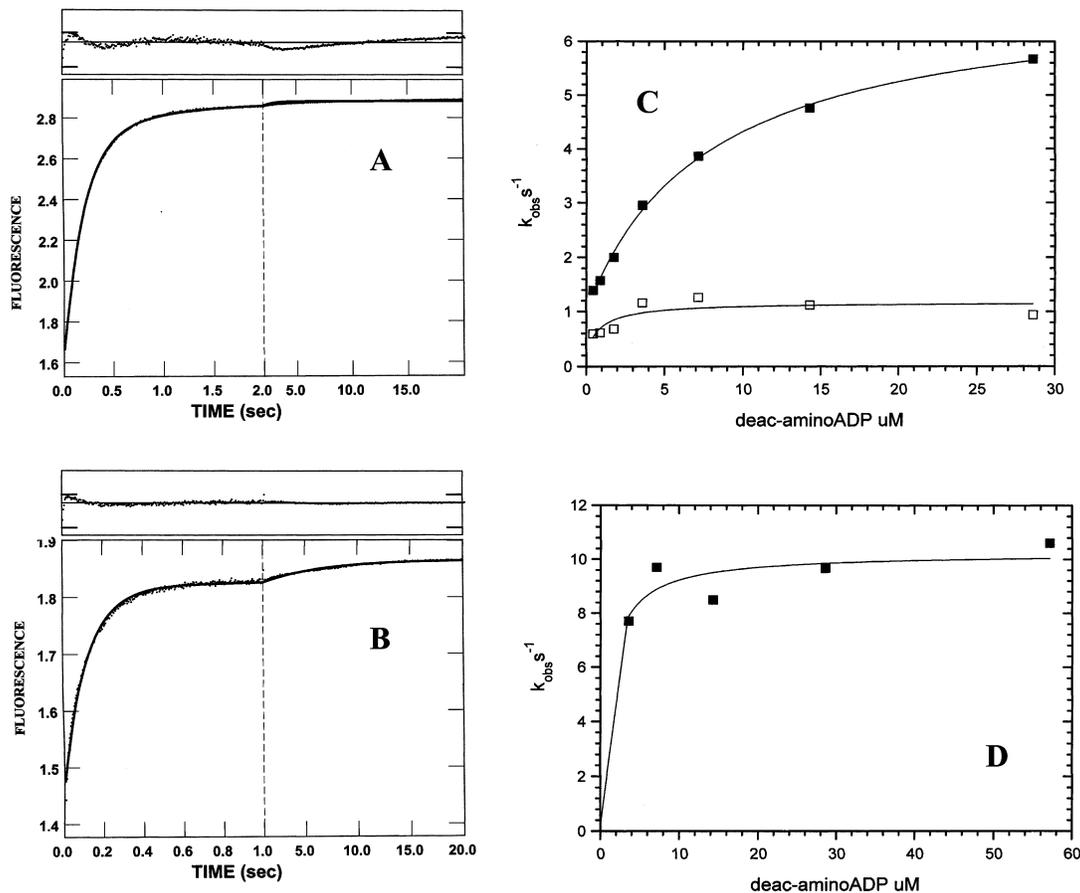
FIGURE 5: Dissociation of ADP from myosinV-S1 and actomyosinV-S1. (A and B) Time course of ADP dissociation from myosinV-S1-ADP (A) and from actomyosinV-S1-ADP (B) using a deac-aminoADP chase. Final concentrations in the flow cell: 0.39 μM myosinV-S1, 4.3 μM ADP, and 14.3 μM deac-aminoADP (A) and 0.14 μM myosinV-S1, 1.42 μM phalloidin actin, 5.7 μM ADP, and 14.3 μM deac-aminoADP (B). The solid line through the data is the best fit to a double exponential equation (normalized amplitudes): $I(t) = 1 - (0.85e^{-4.8t} + 0.15e^{-1.1t}) + C$ for panel A and $I(t) = 1 - (0.93e^{-8.5t} + 0.07e^{-0.2t}) + C$ for panel B. (C and D) The dependence of the observed rate of dissociation of myosinV-S1-ADP (C) and actomyosinV-S1-ADP (D) upon deac-aminoADP concentration. The solid lines through the data in panel C are hyperbolic fits ($\blacksquare$ fast phase and $\square$ slow phase) with maximum rates of 5.9 ± 0.3 s^{-1} for the fast phase and 1.1 ± 0.5 s^{-1} for the slow phase. The dissociation of ADP from actomyosinV-S1-ADP limited the maximum rate of deac-aminoADP binding to 10.1 ± 0.6 s^{-1} (D).
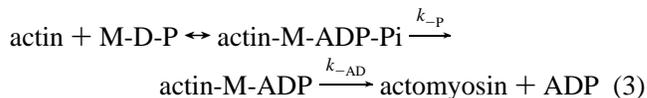
aminoADP-Pi precedes dissociation of deac-aminoADP. Explicit solutions of the kinetic behavior of an ordered mechanism obtained using LaPlace transforms indicate that the relative amplitude of each term is proportional to the other rate constant (*32*).

$$I(t) = I_o(k_1 e^{-k2[actin]t} - k_2[actin]e^{-k1t})/$$
$$(k_1 - k_2[actin]) + C \quad (2)$$

The lag is, therefore, only observed when the values for the two rate constants are similar, that is, $k_1 \sim k_2[actin]$.

   We also used a fluorescently labeled phosphate-binding protein (MDCC-PBP) to measure the rate of Pi dissociation from the actomyosinV-S1-deac-aminoADP-Pi directly. These measurements used double mixing experiments similar to Figure 6A except that 5 μM MDCC-PBP was present in all solutions and the ATP chase was omitted. A complication in this experiment is that MDCC-PBP and deac-aminonucleotides utilize the same fluorescent chromophore and, therefore, have similar excitation and emission wavelengths. It was expected and observed in Figure 6B that a rapid fluorescence increase, produced by Pi dissociation and binding to MDCC-PBP, would be followed by a slower fluorescent decrease produced by the dissociation of deac-aminoADP. The dependence

of the observed rate of phosphate dissociation upon actin concentration in Figure 6C is 7×10^5 M^{-1} s^{-1} when measured with the fluorescent phosphate binding protein (open circles) and 6×10^5 M^{-1} s^{-1} when measured by the lag observed in the deac-aminoADP fluorescence (closed circles). These data indicate that the lag phase observed upon binding myosinV-S1- deac-aminoADP-Pi to actin is produced by phosphate dissociaciation. This interpretation of the lag is supported by experiments measuring deac-aminoADP dissociation from actomyosinV-S1-deacADP in Figure 4F, which are fit very well by a single exponential with no lag. These measurements provide direct evidence that the predominant pathway for product dissociation is ordered dissociation in which phosphate dissociates from actomyosinV-S1-ADP-Pi prior to ADP, as shown in eq 3.

$$\text{actin} + \text{M-D-P} \leftrightarrow \text{actin-M-ADP-Pi} \xrightarrow{k_{-P}}$$
$$\text{actin-M-ADP} \xrightarrow{k_{-AD}} \text{actomyosin} + \text{ADP} \quad (3)$$

   Kinetics of Product Dissociation from ActomyosinV-S1-ADP-Pi. There is no spectroscopic signal associated with the dissociation of unmodified ADP from actomyosinV-S1-ADP-Pi, so direct measurement is not possible. However, the large fluorescence enhancement and rapid and tight
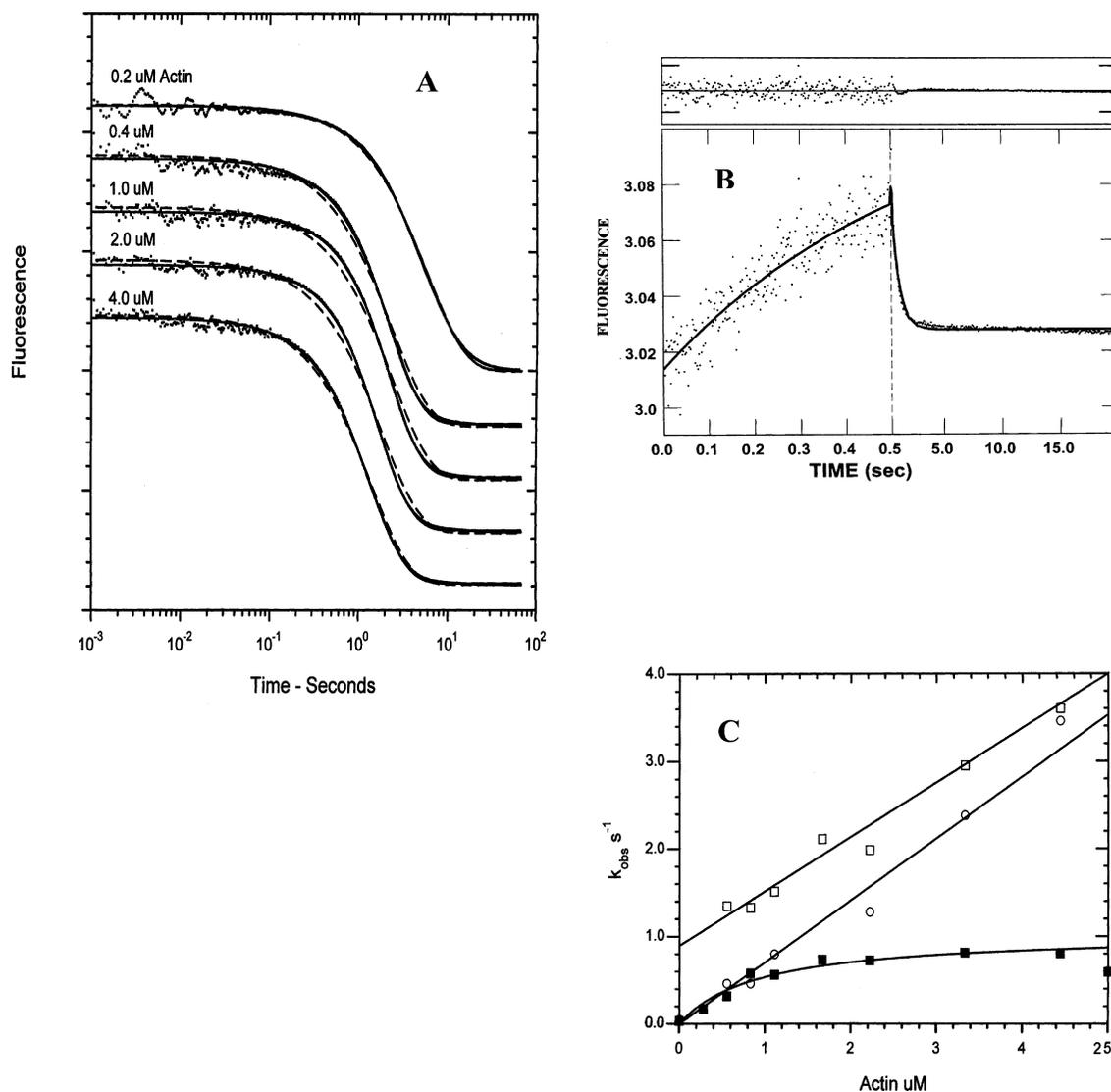
FIGURE 6: Kinetics of product dissociation from actomyosinV-S1-deac-aminoADP-Pi. (A) MyosinV-S1 was mixed with an equimolar concentration of deac-aminoATP, held 20 s in a delay line, and then mixed with phalloidin actin and ATP. The solid lines through the data are fits to $I(t) = I_1e^{-k1t} + I_2e^{-k2t} + C$. The dotted lines are the best fit to a single exponential equation: $I(t) = I_oe^{-kt} + C$. Experimental conditions in the flow cell: 10 mM MOPS, 100 mM KCl, 3 mM MgCl$_2$, 1 mM EGTA, 0.11 μM myosinV-S1, 0.11 μM deac-aminoATP, the indicated concentration of phalloidin-actin, and 111 μM ATP, pH = 7.5 at 20 °C. (B) MyosinV-S1 was mixed with an equimolar concentration of deac-aminoATP, held 20 s in a delay line, and then mixed with 4 μM phalloidin actin in an experiment similar to that discussed in panel A except that all solutions contained 5 μM MDCC-PBP and a phosphate mop (see Experimental Procedures) and ATP was omitted from the actin in the second mix. The solid line through the data is $I(t) = -0.12e^{-2.8t} + 0.1e^{-0.5t} + C$. (C) The solid squares are the slow rate constant, k_1, from panel A, the open squares are the fast component, k_2, in panel A, and the open circles are the fast component, k_1, from panel B.

binding of deac-aminoADP to actomyosinV-S1 makes deac-aminoADP an ideal chase to measure the dissociation of the native products, ADP and phosphate, from actomyosinV-S1-ADP-Pi. In these experiments, myosinV-S1 is first mixed with a 2-fold excess of ATP and held in a delay line for 30 s to generate myosinV-S1-ADP-Pi and then mixed with actin and excess deac-aminoADP. Kinetic modeling of the reaction of ATP with myosinV using the rate constants for ATP binding, 1 μM^{-1} s^{-1}, and steady-state hydrolysis, 0.015 s^{-1} (*15*) indicate that a maximum of 96% myosinV-ADP-Pi occurs at 30 s with 0.4% containing bound ADP and 3.6% with no bound ligands. In practice, the observed kinetics were independent of delay time between 10 and 30 s. The contribution of the fluorescence signal from deac-aminoADP binding to the 3.6% apoenzyme is too small to observe, and almost all (>96%) of the signal is derived from deac-

aminoADP binding after the dissociation of products from actomyosinV-S1-ADP-Pi. The kinetics of the fluorescence increase is poorly fit by a single exponential (dashed lines Figure 7A) but is fit well by two exponentials with opposite amplitudes (solid lines in Figure 7A) in a manner similar to that observed in Figure 6A. The dependence of the observed rates of the two processes upon actin concentration is shown in Figure 7B. The maximum rate of the slow exponential is ~10 s^{-1} at saturating actin (open symbols) with ATP utilized as the substrate. This is faster than that observed in Figure 6B with deac-aminoATP as the substrate as would be expected because of the more rapid dissociation of ADP than deac-aminoADP from actomyosinV-S1, which was previously shown in Figures 4 and 5. At low actin concentrations, the rate of phosphate dissociation is slow and produces the lag. The rate of the lag has a hyperbolic dependence on actin
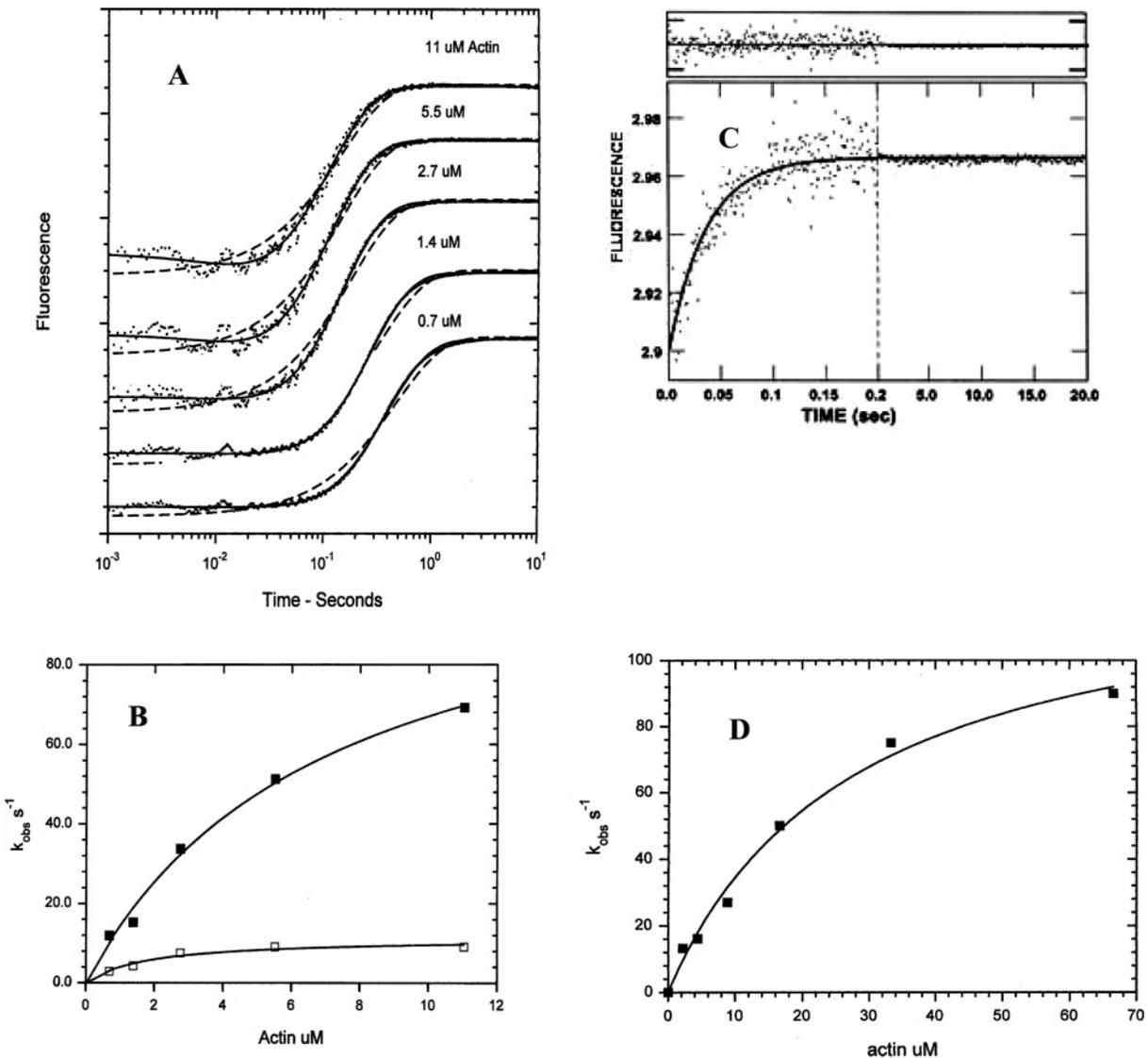
FIGURE 7: Kinetics of phosphate dissociation from actomyosinV-S1-ADP−Pi. (A) MyosinV-S1 was mixed with ATP, held for 30 s, and then mixed with actin and a deac-aminoADP chase. Final concentrations in the flow cell were 0.28 μM myosinV-S1, 0.56 μM ATP, the indicated concentration of actin, and 11.1 μM deac-aminoADP. Solid lines through the data are fit by $I(t) = I_1(1 - e^{-k1t}) + I_2(1 - e^{-k2t}) + C$. The dotted lines are the best fit to a single exponential equation: $I(t) = I_0(1 - e^{-kt})$. (B) Dependence of the rate of the product dissociation steps upon actin concentration. The rate constants determined from the lag in the fluorescence increase varied hyperbolically with the actin concentration with a maximum rate of 80 ± 4 s^{-1} (solid squares) and the rate of the fluorescence increase to a maximum rate of 10 ± 0.4 s^{-1}. (C) Time course of phosphate release. Double mixing stopped-flow experiments using MDCC-PBP were performed as described in the Experimental Procedures. Release of Pi from actomyosinV-S1-deac-aminoADP-Pi was measured by double mixing stopped-flow experiments in which myosinV-S1 was first mixed with ATP, held in a delay line for 30 s, and then mixed with actin to accelerate Pi release. Final concentrations in the flow cell were 0.44 μM myosinV-S1, 0.22 μM ATP, 33.3 μM actin, 1 mM EGTA, 3 mM MgCl$_2$, 10 mM MOPS, 10 μM MDCC-PBP, 0.1 mM 7-methylguanosine, and 0.01 unit/mL purine nucleoside phosphorylase, pH 7.5, 20 °C. (D) Dependence of the rate of phosphate dissociation upon actin concentration. The data are fit by a hyperbolic equation: $k_{obs} = k_{max}/(1 + K_{app}/[\text{actin}])$ when $k_{max} = 131 ± 9$ s^{-1} and $K_{app} = 28 ± 4$ μM.

concentration that reaches a maximal extrapolated rate of ∼80 s^{-1}. However, at high actin concentrations, the observed rate of the lag is only a lower limit of the rate of phosphate dissociation and is limited by the expected rate of 11 μM deac-aminoADP binding to actomyosinV-S1, calculated from the second-order rate constant of deac-aminoADP binding to actomyosinV-S1 (Figure 4). Measuring the rate of phosphate dissociation from the lag at higher concentrations of deac-aminoADP so that deac-aminoADP binding would be faster than the rate of phosphate dissociation was not feasible because of a reduction in the signal-to-noise ratio. The phosphate sensor, MDCC-PBP, was also used to determine the kinetics of phosphate dissociation from actomyosinV-S1-

ADP-Pi in double mixing experiments, as shown in Figure 7C. There is a rapid increase in fluorescence, but the slower decrease that was observed in Figure 6B from deac-aminoADP dissociation is not observed. These data confirm assignment of the rapid increase in fluorescence in Figure 6B to phosphate dissociation and the slower decrease to deac-aminoADP dissociation. The actin dependence of the rate of phosphate dissociation from myosinV-S1-ADP-Pi is shown in Figure 7D. The maximum extrapolated rate of 131 s^{-1} is comparable to previously measured values (*4*, *15*) for phosphate dissociation from actomyosinV-S1-ADP-Pi.

In Vitro Motility. Since the rate of deac-aminoADP dissociation from actomyosinV-S1-deac-aminoADP-Pi is

Table 1: Summary of the Rate Constants for the Mechanism of MyosinV-deac-aminoATP Hydrolysis[a]

$$
\begin{array}{ccccccccc}
 & K_{AT} & & K_{AH} & & K_{-DAP} & & K_{AD} & \\
AM + T & \rightleftharpoons & AM\text{-}T & \rightleftharpoons & AM\text{-}D\text{-}P & \rightarrow & AM\text{-}D & \rightleftharpoons & AM \\
K_A \updownarrow & & K_{TA} \updownarrow & & K_{DPA} \updownarrow & & K_{DA} \updownarrow & & K_A \updownarrow \\
 & K_T & & K_H & & K_{-DP} & & K_D & \\
M + T & \rightleftharpoons & M\text{-}T & \rightleftharpoons & M\text{-}D\text{-}P & \rightarrow & MD & \rightleftharpoons & M
\end{array}
$$

constant	nucleotide	value
k_{AT}	deac-aminoATP	$3.5\ \mu M^{-1}\,s^{-1} \pm 0.2$
k_T	deac-aminoATP	$3.4\ \mu M^{-1}\,s^{-1} \pm 0.3$
k_D	deac-aminoADP	$5.7\ \mu M^{-1}\,s^{-1} \pm 0.2$
k_{AD}	deac-aminoADP	$5.4\ \mu M^{-1}\,s^{-1} \pm 0.1$
k_{-D}	deac-aminoADP	$0.49\ s^{-1} \pm 0.02$
k_{-D}	ADP	$5.9\ s^{-1} \pm 1.0$
k_{-AD}	deac-aminoADP	$0.52\ s^{-1} \pm 0.02$
k_{AD}	ADP	$10.6\ s^{-1} \pm 1.0$
$1/K_D$	deac-aminoADP	$0.09\ \mu M \pm 0.01$
$1/K_{AD}$	deac-aminoADP	$0.09\ \mu M \pm 0.01$

[a] Subscripts to the equilibrium constants denote ligands bound to myosin (M): A = actin; T = ATP; D = ADP; P = P$_i$; and H = hydrolysis. The last subscript is the ligand associating or dissociating (indicated by − preceding the subscript). For example, K_{-DAP} is phosphate dissociating from actomyosinV-S1-ADP-Pi.

∼20 times slower than the dissociation of ADP, we expected that the velocity of motility would be also reduced to a similar extent in the presence of deac-aminoATP. Initial attempts to measure the velocity with the Cell-trak motion analysis system for deac-aminoATP were not successful because the slower velocity required longer recording times that resulted in significant photobleaching. The problem was circumvented by using time lapse (20 ms exposure measurements every 100 s) and analyzing the images with the Metamorph software. There is a hyperbolic dependence of the velocity on the deac-aminoATP concentration with a maximum rate of 8.4 ± 0.7 nm (Figure 8). In a control experiment at saturating ATP, the velocity was 200 nm/s as previously observed (*12*), which is ∼20 times more rapid than that measured here with deac-aminoATP.
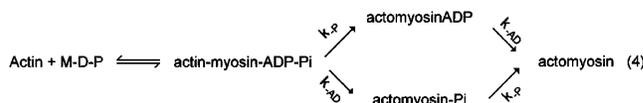
DISCUSSION

We have determined rate constants of elementary steps of the kinetic mechanism of the hydrolysis of the fluorescent ATP analogue, deac-aminoATP, by myosinV-S1 using stopped-flow fluorescence. The fluorescence emission of deac-aminoATP increases ∼20-fold upon binding to myosinV-S1. Excellent signal-to-noise ratios can be obtained with concentrations as low as 20 nM myosinV sites in a stopped-flow cell with substoichiometric nucleotide or a ratio of 100:1 of deac-aminonucleotide to sites in chase experiments at 100 nM myosinV-S1. A summary of the rate constants is provided in Table 1. Deac-aminoATP binds to myosinV-S1 and to actomyosinV-S1 with a rate of $3 \times 10^6\ M^{-1}\,s^{-1}$, which is 3 times the rate of ATP and mantATP binding (*15, 17*). The only significantly altered first-order step is the rate of dissociation of deac-aminoADP, which is 10-fold slower than the rate of ADP dissociation from myosinV-S1 and 20-fold for actomyosinV-S1. The 20-fold slower rate measured for the dissociation of deac-aminoADP is consistent with the ∼20-fold reduction in the motility of myosinV measured with deac-aminoATP as the substrate as compared to ATP.

The rate and equilibrium constants of deac-aminoADP binding to myosinV-S1 are the same in the presence and in the absence of actin, which suggests that the conformation of the ADP binding site to myosinV-S1 is not significantly affected by actin binding. The kinetics of dissociation of deac-aminoADP from both myosinV-S1 and actomyosinV-S1 are very accurately fit by single exponential fluorescence changes, which suggests that only a single molecular species of myosin-deac-aminoADP or actomyosin-deac-aminoADP is present. However, the kinetics of deac-aminoADP binding to myosinV-S1 and actomyosinV-S1 are best fit by biphasic kinetics, which include a fast component that is proportional to deac-aminoADP concentration and a small, slow (∼1 s^{-1}) change that comprises 5−10% of the total signal. In principle, the slow signal might be produced by dissociation of ADP that remained bound to the active site after purification of the enzyme. However, the same, slow component was also observed upon mixing myosinV-S1-ADP with deac-aminoADP, which suggests that it is the result of an isomerization following the formation of an initial myosinV-S1-deacADP complex.

Here, we have shown that phosphate dissociation can be observed either from the lag in the fluorescent signal produced by deac-aminoADP dissociation from actomyosinV-S1-deac-aminoADP-Pi using ATP as a chase (Figure 6) or from the lag produced by product dissociation from actomyosinV-S1-ADP-Pi using deac-aminoADP as the chase (Figure 7). The actin dependence of the rate of Pi dissociation from actomyosinV-S1-deac-aminoADP-Pi was also directly measured in double mixing experiments using the phosphate sensor MDCC-PBP (Figure 6).

Although it has been widely assumed that the mechanism of product dissociation is ordered because phosphate dissociates more rapidly than ADP from actomyosinV-S1-ADP-Pi, it has not been directly demonstrated. Faster dissociation of phosphate is also consistent with a random mechanism of product dissociation shown in eq 4 in which phosphate dissociates more rapidly but is not ordered.

$$
\begin{array}{ccccc}
 & & \text{actomyosinADP} & & \\
 & \nearrow^{k_{-P}} & & \searrow^{k_{-AD}} & \\
\text{Actin} + \text{M-D-P} \rightleftharpoons \text{actin-myosin-ADP-Pi} & & & & \text{actomyosin} \quad (4) \\
 & \searrow_{k_{-AD}} & & \nearrow^{k_{-P}} & \\
 & & \text{actomyosin-Pi} & &
\end{array}
$$

The lag in the fluorescence increase produced by a deac-aminoADP chase of actomyosinV-S1-ADP-Pi could, in principle, be used to distinguish between ordered and random mechanisms of product dissociation. Modeling of the reaction shows that at saturating actin concentrations (∼50 μM), the fluorescence signal produced by a random mechanism is very accurately single exponential as compared to the signal produced by an ordered mechanism, which is calculated to have a small but significant deviation from a single exponential in the form of a lag. Such an experiment would also have to be performed at a high enough deac-aminoADP concentration (∼100 μM) to make binding of the chase significantly faster than either of the product dissociation steps. Although the rate of deac-aminoADP binding is fast enough so that there is not a significant lag at the lower concentrations of actin (<3 μM), the maximum rate of the lag (80 s^{-1}) is limited by the rate of deac-aminoADP binding to actomyosinV-S1. However, at 100 μM deac-aminoADP, the signal-to-noise ratio is not good enough to make the measurement at the required level of precision. Nevertheless,
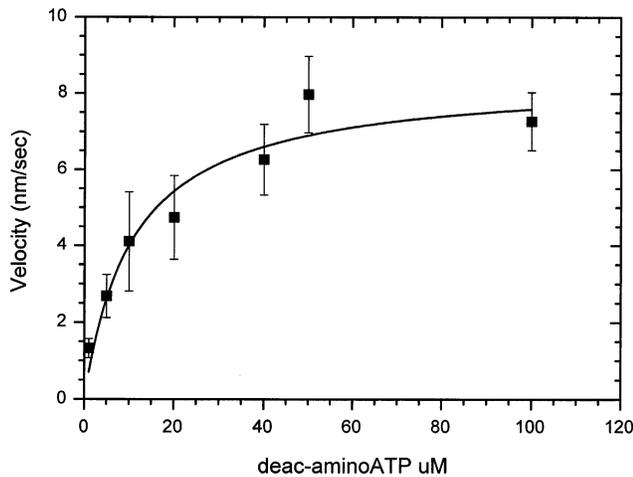
FIGURE 8: Dependence upon deac-aminoATP concentration of the velocity of rhodamine−phalloidin labeled actin gliding over myosinV-HMM. The data were fit to a hyperbolic curve with a maximum velocity of 8.4 ± 0.7 ηm/s and a K_{app} of 11 ± 3 μM. Experimental conditions are described in the Experimental Procedures. Motility assays were carried out at 30 °C.

the observed rate obtained at subsaturating actin concentrations provides evidence of an ordered mechanism of product dissociation from actomyosinV-S1-ADP-Pi, in which rapid dissociation of phosphate preceding slower dissociation of ADP is the principal pathway of product dissociation from actomyosinV-S1-ADP-Pi.

ACKNOWLEDGMENT

REFERENCES

1. Rosenfeld, S. S., and Taylor, E. W. (1984) The ATPase mechanism of skeletal and smooth muscle acto-subfragment 1, *J. Biol. Chem. 259*, 11908−11919.
2. Smith, S. J., and White, H. D. (1985) Kinetic mechanism of 1-N^6-etheno-2-aza-ATP hydrolysis by bovine ventricular myosin subfragment 1 and actomyosin subfragment 1. The nucleotide-binding steps, *J. Biol. Chem. 260*, 15146−15155.
3. Woodward, S. K., Eccleston, J. F., and Geeves, M. A. (1991) Kinetics of the interaction of 2′(3′)-O-(N-methylanthraniloyl)-ATP with myosin subfragment 1 and actomyosin subfragment 1: characterization of two acto-S1-ADP complexes, *Biochemistry 30*, 422−430.
4. Rosenfeld, S. S., and Sweeney, H. L. (2004) A model of myosin V processivity, *J. Biol. Chem. 279*, 40100−40111.
5. Oiwa, K., Eccleston, J. F., Anson, M., Kikumoto, M., Davis, C. T., Reid, G. P., Ferenczi, M. A., Corrie, J. E., Yamada, A., Nakayama, H., and Trentham, D. R. (2000) Comparative single molecule and ensemble myosin enzymology: sulfoindocyanine ATP and ADP derivatives, *Biophys. J. 78*, 3048−3071.
6. Webb, M. R., Reid, G. P., Munasinghe, V. R., and Corrie, J. E. T. (2004) A series of related nucleotide analogues that aids optimization of fluorescence signals in probing the mechanism of P-loop ATPases, such as actomyosin, *Biochemistry 43*, 14463−14471.
7. Vale, R. D. (2003) Myosin V motor proteins: marching stepwise towards a mechanism, *J. Cell Biol. 163*, 445−450.
8. Mehta, A. D., Rock, R. S., Rief, M., Spudich, J. A., Mooseker, M. S., and Cheney, R. E. (1999) Myosin-V is a processive actin-based motor, *Nature 400*, 590−593.
9. Cheney, R. E., O'Shea, M. K., Heuser, J. E., Coelho, M. V., Wolenski, J. S., Espreafico, E. M., Forscher, P., Larson, R. E., and Mooseker, M. S. (1993) Brain myosin-V is a two-headed unconventional myosin with motor activity, *Cell 75*, 13−23.
10. Sellers, J. R. (1999) *Myosins*, Sheterline, P., Ed., Oxford University Press; Oxford, U.K.
11. Watterson, D. M., Sharief, F., and Vanaman, T. C. (1980) The complete amino acid sequence of the Ca^{2+}-dependent modulator protein (calmodulin) of bovine brain, *J. Biol. Chem. 255*, 962−975.
12. Walker, M. L., Burgess, S. A., Sellers, J. R., Wang, F., Hammer, J. A. III, Trinick, J., and Knight, P. J. (2000) Two-headed binding of a processive myosin to F-actin, *Nature 405*, 804−807.
13. Sakamoto, T., Wang, F., Schmitz, S., Xu, Y., Xu, Q., Molloy, J. E., Veigel, C., and Sellers, J. R. (2003) Neck length and processivity of myosin V, *J. Biol. Chem. 278*, 29201−29207.
14. Rief, M., Rock, R. S., Mehta, A. D., Mooseker, M. S., Cheney, R. E., and Spudich, J. A. (2000) Myosin-V stepping kinetics: a molecular model for processivity, *Proc. Natl. Acad Sci. U.S.A. 97*, 9482−9486.
15. De La Cruz, E. M., Wells, A. L., Rosenfeld, S. S., Ostap, E. M., and Sweeney, H. L. (1999) The kinetic mechanism of myosin V, *Proc. Natl. Acad. Sci. U.S.A. 96*, 13726−13731.
16. Veigel, C., Wang, F., Bartoo, M. L., Sellers, J. R., and Molloy, J. E. (2002) The gated gait of the processive molecular motor, myosin V, *Nat. Cell. Biol. 4*, 59−65.
17. Trybus, K. M., Krementsova, E., and Freyzon, Y. (1999) Kinetic characterization of a monomeric unconventional myosin V construct, *J. Biol. Chem. 274*, 27448−27456.
18. Lymn, R. W., and Taylor, E. W. (1971) Mechanism of adenosine triphosphate hydrolysis by actomyosin, *Biochemistry 10*, 4617−4624.
19. White, H. D., and Taylor, E. W. (1976) Energetics and mechanism of actomyosin adenosine triphosphatase, *Biochemistry 15*, 5818−5826.
20. Hiratsuka, T. (1983) New ribose-modified fluorescent analogues of adenine and guanine nucleotides available as substrates for various enzymes, *Biochim. Biophys. Acta 742*, 496−508.
21. Wang, F., Chen, L., Arcucci, O., Harvey, E. V., Bowers, B., Xu, Y., Hammer, J. A., III, and Sellers, J. R. (2000) Effect of ADP and ionic strength on the kinetic and motile properties of recombinant mouse myosin V, *J. Biol. Chem. 275*, 4329−4335.
22. Gill, S. C., and von Hippel, P. E. (1989) Calculation of protein extinction coefficients from amino acid sequence data, *Anal. Biochem. 182*, 319−326.
23. Spudich, J. A., and Watt, S. (1971) The regulation of rabbit skeletal muscle contraction. I. Biochemical studies of the interaction of the tropomyosin−troponin complex with actin and the proteolytic fragments of myosin, *J. Biol. Chem. 246*, 4866−4871.
24. Brune, M., Hunter, J. L., Corrie, J. E. T., and Webb, M. R. (1994) Direct, real-time measurement of rapid inorganic phosphate release using a novel fluorescent probe and its application to actomyosin subfragment 1 ATPase, *Biochemistry 33*, 8262−8271.
25. White, H. D., Belknap, B., and Webb, M. R. (1997) Kinetics of nucleoside triphosphate cleavage and phosphate release steps by associated rabbit skeletal actomyosin, measured using a novel fluorescent probe for phosphate, *Biochemistry 36*, 11828−11836.
26. Nixon, A. E., Hunter, J. L., Bonifacio, G., Eccleston, J. F., and Webb, M. R. (1998) Purine nucleoside phosphorylase: its use in a spectroscopic assay for inorganic phosphate and for removing inorganic phosphate with the aid of phosphodeoxyribomutase, *Anal. Biochem. 265*, 299−307.
27. Homsher, E., Wang, F., and Sellers, J. R. (1992) Factors affecting movement of F-actin filaments propelled by skeletal muscle heavy meromyosin, *Am. J. Physiol. 262*, 714−723.
28. Eccleston, J. F., Hutchinson, J. P. and White, H. D. (2001) Stopped flow techniques in protein−ligand interactions, in *Structure and Spectroscopy, Practical Approach Series* (Harding, S. E. C. B., Ed.) pp 201−237, Oxford University Press, New York.
29. Griffiths, P. J., Guth, K., Kuhn, H. J., and Ruegg, J. C. (1980) ATPase activity in rapidly activated skinned muscle fibres, *Pfluegers Arch. 387*, 167−73.
30. De La Cruz, E. M., Sweeney, H. L., and Ostap, E. M. (2000) ADP inhibition of myosin V ATPase activity, *Biophys. J. 79*, 1524−1529.
31. Hannemann, D. E., Cao, W., Olivares, A. O., Robblee, J. P., and De La Cruz, E. M. (2005) Magnesium, ADP, and actin-binding linkage of myosin V: evidence for multiple myosin V-ADP and actomyosin V-ADP states, *Biochemistry 44*, 8826−8840.
32. Zhang, X. Z., Strand, A., and White, H. D. (1989) A general pre-steady-state solution to complex kinetic mechanisms, *Anal. Biochem. 176*, 427−431.